Pergamon

Geochimica et Cosmochimica Acta, Vol. 64, No. 5, pp. 897–910, 2000

0016-7037/00 $20.00 + .00

PII S0016-7037(99)00349-X

Sulfate reduction and methane oxidation in continental margin sediments influenced by irrigation (South-East Atlantic off Namibia)

Henrik Fossing,[1,*] Timothy G. Ferdelman,[2] and Peter Berg[3]

[1]Department of Lake and Estuarine Ecology, National Environmental Research Institute, Vejlsøvej 25, POB 314, DK-8600 Silkeborg, Denmark
[2]Max Planck Institute for Marine Microbiology, Celsius Strasse 1, D-28359 Bremen, Germany
[3]Department of Environmental Sciences, University of Virginia, Charlottesville, VA 22903, USA

(*Received January* 11, 1999; *accepted in revised form September* 7, 1999)

Abstract—Sulfate reduction rates (SRR) and concentrations of SO_4^{2-}, H_2S, pyrite sulfur, total sulfur, CH_4, and organic carbon were measured with high depth resolution through the entire length of the SO_4^{2-}-zone and well into the CH_4-zone at two continental slope stations in the eastern South Atlantic (Benguela upwelling area). The sediments were characterized by a high organic carbon content of approx. 7.5% at GeoB 3703 and 3.7% at GeoB 3714. At GeoB 3703 SO_4^{2-} concentrations decreased linearly with depth to about 40 μM at the sulfate-methane transition zone (SMT) at 3.5 m, while at GeoB 3714, SO_4^{2-} remained at sea water concentration in the top 2 m of the sediment and then decreased linearly to about 70 μM at the SMT at 6 m. Direct rate measurements of SRR ($^{35}SO_4^{2-}$) showed that the highest SRR occurred within the surface 3–5 cm with peak rates of up to 20 and 7 nmol SO_4^{2-} cm^{-3} day^{-1} at GeoB 3703 and GeoB 3714, respectively. SRR decreased quasi-exponentially with depth at GeoB 3703 and the cumulative SRR over the length of the SO_4^{2-} zone resulted in an areal SRR (SRR_{area}) of 1114–3493 μmol m^{-2} day^{-1} (median value: 2221 μmol m^{-2} day^{-1}) at GeoB 3703 with more than 80% of the total sulfate reduction proceeding in the top 30 cm sediment. At GeoB 3714 SRR exhibited more scatter with a cumulative SRR_{area} of 398–1983 μmol m^{-2} day^{-1} (median value: 1251 μmol m^{-2} day^{-1}) and with >60% of the total sulfate reduction occurring below a depth of 30 cm due partially to a deeply buried zone of sulfate reduction located between 3 and 5 m depths. SRR peaks were also observed in SMT of both cores, ostensibly associated with methane oxidation, but with rates about 10 times lower than at the surface. Modeled SRR balanced both methane oxidation rates and measured SRR within the SMT, but severely underestimated by up to 89% the total SRR_{area} that were obtained from direct measurements. Modeled and measured SRR were reconciled by including solute transport by irrigation described by a non-local pore water exchange function (α) which had values of up to 0.3 $year^{-1}$ in the top sediment, and decreased exponentially to zero (i.e., no irrigation) at 2–3 meters (i.e., above SMT). These results suggested that co-existing sulfate reduction processes and linear SO_4^{2-}-gradients can be maintained by a non-local transport mechanism such as irrigation, by which pore water in tubes or burrows is exchanged with bottom waters by activities of tube-dwelling animals, or some similar physical transport phenomenon (i.e., bubble ebullition). Further support for an irrigation mechanism was found in the observations of open tubes of up to 8 mm (ID) at depths down to 6 m, which also contained fecal pellets, indicating that these tubes were or had been inhabited.

1. INTRODUCTION

Sulfate is reduced to H_2S by sulfate reducing bacteria primarily through the oxidation of organic matter (Widdel, 1988). Sulfate concentrations in marine pore waters therefore gradually decrease with depth creating a concave-down SO_4^{2-} profile (Berner, 1964; Jørgensen, 1983). Before the SO_4^{2-} pool becomes completely exhausted and sulfate reduction (SR) ceases CH_4 builds up in the sediments and stimulates SR in the bottom of the SO_4^{2-} zone (Devol et al., 1984; Alperin and Reeburgh, 1985; Iversen and Jørgensen, 1985; Hoehler et al., 1994; Niewöhner et al., 1998).

A common feature of many continental margin sediments is that SO_4^{2-} at sea water concentration penetrates several meters down into the sediments as seen from the Congo Fan and the upwelling areas of the eastern South Atlantic (Pimenov et al., 1993; Schulz et al., 1994; Niewöhner et al., 1998; Pruysers, 1998), the Amazon shelf (Blair and Aller, 1995; Aller et al., 1996) and the north west Atlantic, Carolina Rise (Borowski et al., 1997). Whereas, there appears to be little or no SR in the upper meters of the sediment at these stations (as deduced from the lack of gradients in SO_4^{2-} concentration over depth), SR appears to commence at greater depths linked to the oxidation of CH_4 (Schulz et al., 1994; Niewöhner et al., 1998; Burns, 1998). The apparent lack of SR from the surface sediment to near the bottom of the SO_4^{2-} zone has been previously attributed to the recalcitrant characteristics of the organic matter towards SR or simply to an absence of sulfate reducing bacteria (Jahnke et al.,1989).

In February 1996, during Meteor Cruise M 34/2 we visited two stations in the eastern South Atlantic upwelling area, GeoB 3703 (1372 m) and GeoB 3714 (2060 m), of which the latter had already been subject of various studies earlier (Wefer et al., 1988; Schulz et al., 1994). At both stations we measured sulfate reduction rates (SRR) by use of radio labeled sulfate ($^{35}SO_4^{2-}$) (Jørgensen, 1978) but we also modeled SRR and CH_4 oxidation from the concentration profiles of SO_4^{2-} and CH_4, respectively (Berg et al., 1998). The $^{35}SO_4^{2-}$ labeling technique has the advantage that it allows SRR measurements with a high depth

*Author to whom correspondence should be addressed (HFO@dmu.dk).

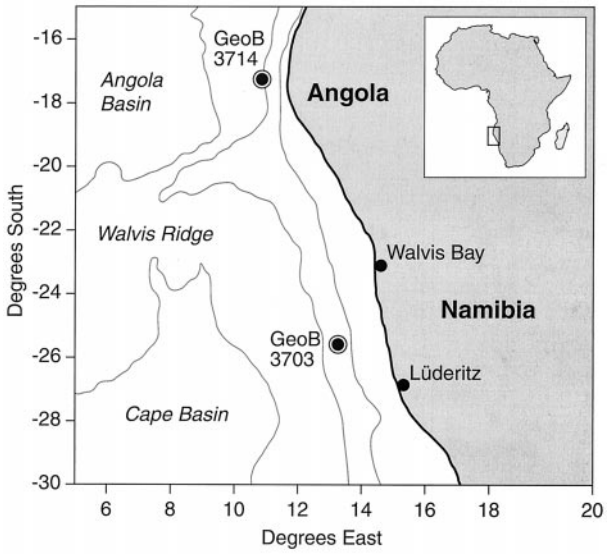

Fig. 1. Map of the south east Atlantic study area off Namibia and Angola showing Station GeoB 3703 at 1373 m (13°13.8′E; 25°31.1′S) and Station GeoB 3714 at 2065 m (10°59.8′E; 17°09.6′S). Bottom water temperature: 4°C.

resolution and even at non-steady state situations. Further, $^{35}SO_4^{2-}$ injections allow exact SRR determination in both bioturbated and irrigated sediments, activities that tend to straighten out the gradient change of the SO_4^{2-} concentration profile and hence underestimate SRR if modeled from such profiles. Thus, $^{35}SO_4^{2-}$ labeling has been applied both in near shore sediments where no gradient change in sulfate concentrations are observed (see for example Edenborn et al., 1987; Jørgensen, 1989; Fossing and Jørgensen, 1990; Thamdrup et al., 1994; Ferdelman et al., 1997) and in continental margin and deep-sea sediments (Battersby et al., 1985; Rowe and Howarth, 1985; Fossing, 1990; Heggie et al., 1990; Devol and Christensen, 1993; Pimenov et al., 1993; Parkes et al., 1994; Ferdelman et al., 1999).

Our scientific interest was to sample sediment at the two stations to:

1. demonstrate that bacteria were actively reducing SO_4^{2-} also in the surface sediments with no SO_4^{2-} gradient;
2. demonstrate that CH_4 oxidation at the bottom of the SO_4^{2-} zone was the major process through which sulfate was reduced at these depths; and
3. explain the disagreement between the observation of SR in a zone of non-changing SO_4^{2-} gradient given that we observed SR above the sulfate-methane transition zone (SMT).

2. MATERIAL AND METHODS

Sediment from the continental slope off Namibia was sampled from the R/V Meteor (Hamburg) by use of a 17.25 m long (12 cm ID) gravity corer (GC) and a multiple corer (MuC, each sediment core > 30 cm long, 10 cm ID). Gravity cores of 950 cm and 1297 cm length were obtained, respectively from GeoB 3703 and GeoB 3714, see Figure 1. As gravity coring disturbs the surface sediment, SRR and related parameters in the top 30 cm of the sediment were measured in the undisturbed surface sediment obtained from MuC coring.

2.1. Sub-Sampling the Gravity Core

The GC was immediately processed after retrieval by cutting the core liners into one meter sections, followed by capping and storage in a 4°C cold room. Sub-sampling of the one meter GC-sections was performed in a refrigerated on-board laboratory at 4°C, slowly pushing the sediment out of the upright core liner. Sediment was sub-sampled at 10–20 cm intervals, excluding the upper 5 cm and lower < 10 cm of each 1 m core section. From the center part of each section we sampled sub-cores of 5–7 cm length (12 mm, ID) into 5 ml plastic syringes (PS) with the lure lock end cut off or into glass barrels (GB) of the same size fitted with a syringe piston. The sediment directly below (i.e. 7–9 cm) was sub-sampled for pore water (PW) and solid phase analyses.

2.2. Handling of Sub-Samples from the Gravity Core

2.2.1. Sulfate reduction

Three GB sub-cores were injected with 10 μl, 400 kBq carrier-free $^{35}SO_4^{2-}$ (Amersham). The needle was slowly pulled back through the center of the sediment core while the tracer was added from the far end of the incubation syringe. The GB was then capped with a butyl rubber stopper. The three $^{35}SO_4^{2-}$ labeled sediment cores were incubated at in situ temperature, in the dark and under an argon atmosphere for 24, 48, and 72 hours, respectively. Technically it was not possible to perform the incubations at in situ pressure and the measured SRR should be seen in the light of this. The problem of pressure effects on deep-sea microbial processes has occupied deep-sea scientists for decades. However, observations on decompression effects on process rates are often in conflict showing both increased rates (Jannasch and Taylor, 1984; Rowe and Deming, 1985), decreased rates (Bianchi and Garcia, 1993), or no effect at all, particularly for sulfate reduction rate measurements (Martens et al., 1998; Boetius et al., in press). Based on studies thus far (see Ferdelman et al. (1999) for a more detailed discussion), we anticipate that we have obtained accurate in situ SRR.

We terminated the SRR-incubations by mixing the sediment with 20% zinc acetate (ZnAc—1:1; vol.:vol.). For every fifth sub-section a blank (i.e., time zero) sample was also done, preserving the sediment with ZnAc before the $^{35}SO_4^{2-}$ tracer was added. All radio-labeled ZnAc-preserved samples were stored frozen. Bacterial sulfate reduction rate was quantified from the reduction of $^{35}SO_4^{2-}$ into total reducible inorganic sulfur (TRIS = $H_2^{35}S$, $Fe^{35}S$, $Fe^{35}S_2$, and $^{35}S^o$) and was determined using a modified version of the one-step acidic Cr-II method (Fossing and Jørgensen, 1989). The modification of the method involved the use of two 7 ml ZnAc-solution traps in series rather than a single 10 ml trap. The liberated $H_2^{35}S$ was entirely trapped in the first trap as $Zn^{35}S$ and the entire content of the trap was used for scintillation counting. A Canberra-Packard 2400 TR liquid scintillation counter (with Pakard Ultima Gold XR scintillation fluid) was used to determine the $Zn^{35}S$ and $^{35}SO_4^{2-}$ radioactivity, the latter separated from the sediment and the reduced inorganic solid sulfur compounds by centrifugation.

The sulfate reduction rate was calculated from the fraction of reduced sulfur produced during incubation and the in situ sulfate concentration,

$$\mathrm{SRR} = \frac{a-b}{A+a}[SO_4^{2-}]\frac{1}{d}\cdot 1.06 \text{ nmol cm}^{-3}\text{ day}^{-1} \quad (1)$$

where, *a* is the radioactivity of the reduced sulfur compounds per volume sediment, *b* is the radioactivity in the ZnAc trap after chromium reduction of the time zero sample of an equivalent volume (i.e., the carry over of non-reduced ^{35}S to the ZnAc trap, also named "the blank value"), A is the radioactivity of the sulfate per volume sediment after incubation, $[SO_4^{2-}]$ is the sulfate concentration (nmol cm^{-3}), d is the incubation time in days, and 1.06 is the isotopic fractionation factor (Jørgensen and Fenchel, 1974).

Determination of the blank value *b* in the GC and MuC resulted in values of 138 ± 75 cpm per volume sediment (n = 16) for the GC sampled sediment and 136 ± 60 cpm per volume sediment (n = 12) for the MuC. No correlation with depth, sample site or sample handling was noted. Thus, sulfate reduction was only considered detectable when (a − b) exceeded the double standard deviation of the blank value, i.e., 150 cpm and 120 cpm for the GC and MuC sampled

sediment, respectively. In addition to the double standard deviation of the blank value, the detection limit (SRR_{lim}) determined by injection of 400 kBq $^{35}SO_4^{2-}$ also depended on the SO_4^{2-} concentration and incubation length,

$$SRR_{lim} = f[SO_4^{2-}]\frac{1}{d} \cdot 1.06 \text{ nmol cm}^{-3} \text{ day}^{-1} \quad (2)$$

where, f is (150/24 000 000 =) 6.25×10^{-6} for the GC samples and 5×10^{-6} for the MuC samples assuming a 100% counting efficiency. The values of $[SO_4^{2-}]$ and d are defined above.

2.2.2. Methane

Approximately 5 cm^3 of sediment were sub-sampled using a GB syringe and immediately transferred to a 50 ml serum bottle containing 10 ml $HgCl_2$ (1.4 g $litre^{-1}$) in a 7% NaCl solution. The vial was immediately sealed, crimp capped and vigorously shaken for 1 min to break up the sediment and finally stored at 4°C until concentration determination onboard. Concentrations were measured in 25 μl of headspace gas using a Varian 3400 gas chromatograph equipped with a splitless injector, a capillary column (30 m $\times$ 0.544 mm) and a flame ionization detector. N_2 served as carrier gas with a flow rate of 6 ml min^{-1} and methane eluted at 1.8 min. The CH_4 peak was quantified by comparisons with a 5 point linear calibration curve and corrected for a background of 25–31 μM CH_4 (air in core-sampling cold room).

2.2.3. Pore water concentrations of SO_4^{2-} and H_2S

Approximately 20 cm^3 of sediment was sub-sampled from the GC and transferred to a pneumatic pore water squeezer. Pore water was collected directly into an argon-washed 5 ml glass syringe by pressure filtration through a 0.45 μm membrane filter. In an argon filled glove bag a known volume of PW was preserved in 1.00 ml 2% $ZnCl_2$ and frozen. Sulfate concentrations $>$ 5 mM were determined on 100 fold diluted and filtered PW samples by non-suppressed anion exchange chromatography (Waters 510 HPLC Pump; Waters IC-Pak 50 $\times$ 4.6 mm anion exchange column; and Waters 430 Conductivity detector). Isophtalic acid (1 mM) in 10% methanol (pH 4.6) was used as eluant. Sulfate concentrations $<$ 5 mM were determined on undiluted but filtered PW samples by suppressed ion chromatography (Sykam, Gilching, Germany) with a detection limit of 40 μM and 70 μM at GeoB 3703 and GeoB 3714, respectively. Dissolved sulfide preserved as ZnS were determined by the methylene blue method as described by Cline (1969).

2.2.4. Solid phases (S^o, FeS, and FeS_2)

About 40 cm^3 sediment was preserved in 40 ml of a 20% ZnAc-solution (w/v) and frozen for later determination of solid phase reduced inorganic sulfur. Elemental sulfur (S^o) was extracted from 200 mg of the ZnAc-preserved sediment using 10 ml of HPLC grade methanol. Elemental sulfur (as S_8) was measured by reverse-phase HPLC (Sykam S2000 pump; a 120 $\times$ 4.6 mm Zorbax-ODS column, and a Linear UV 200 detector set at 265 nm). S_8 eluted at 3.7 min. with 100% methanol as an eluant at 1 ml min^{-1}. Acid Volatile Sulfide (AVS = H_2S + FeS) and Chromium Reducible Sulfur (CRS = FeS_2 + S^o) were determined on 500 mg of the ZnAc-preserved sediment using the two-step acid Cr-II method (Fossing and Jørgensen, 1989). The pore water concentration of H_2S was subtracted from the AVS concentration and the S^o-concentration from the CRS-concentration to give concentrations of FeS sulfur and pyrite (FeS_2) sulfur, respectively.

2.2.5. Density, porosity, total S and total organic C

An approx. 5 cm^3 GC sub-core was sampled with a plastic syringe from each depth interval. The syringe was closed with a butyl rubber stopper and stored at 4°C. Density was determined from weight and volume and porosity from weight loss after heating the sediment at 80°C until complete dryness. Densities and porosities were used to recalculate rates and concentrations from weight to volume.

Total sulfur (TS) was determined on the dried samples using a Fisons CHNS-O 1500 Elemental Analyzer. Samples were first washed three times with distilled water to remove sea water sulfate. Vanadium pentaoxide was then added to the samples in order to assure complete recovery of TS. Total organic carbon (TOC) was determined on the same instrument after pre-treating sediment sub-samples (pre-weighed into Ag foil combustion cups) with drops of 1M HCl and drying at 60°C.

2.3. Sub-Sampling and Handling of Sediment from the Multiple Corer

A multiple corer was employed to retrieve undisturbed sediment from the sea floor and $>$30 cm surface sediment from thee MuC was sub-sampled into 40 cm long acrylic core liners (26 mm ID). Sediment for SRR measurements was sampled in triplicate into core liners equipped with one cm separated silicone stoppered ports (2 mm ID) for $^{35}SO_4^{2-}$ injection. Also sub-cores for SO_4^{2-} concentration and density/porosity were immediately sampled. All sub-cores were stored at 4°C until further handling.

2.3.1. Sulfate reduction rate measurement

Three sub-cores were injected at 1 cm intervals with approximately 5 μl of 80 kBq ml^{-1} $^{35}SO_4^{2-}$ carrier-free tracer (Amersham) using the whole-core $^{35}SO_4^{2-}$ method developed by Jørgensen (1978). Overlying water was removed to allow a natural oxygen penetration to the surface sediments, as dissolved O_2 concentrations in the overlying water at all stations was approximately 200 μM (Schulz et al., 1996). The sub-cores were incubated in the dark at temperatures (but not pressures) reflecting in situ conditions. After 8 to 12 h the bacterial activity was halted by slicing the cores at 1 cm intervals into an equal volume of 20% ZnAc-solution (w/v) and freezing. ^{35}S incorporation into TRIS was determined using the one-step acidic Cr-II method (Fossing and Jørgensen, 1989) as described above.

2.3.2. Sulfate concentration, density and porosity

The sub-sampled sediment was stored as whole cores at $-$20°C and 4°C for SO_4^{2-} concentration measurements and density/porosity determination, respectively. Sulfate concentrations were measured on shore after the frozen cores were sliced into 1 or 4 cm sections and thawn. The pore water was separated by centrifugation and filtration through a 0.40 μm syringe filter and SO_4^{2-} concentration was measured as described above. The 4°C sub-cores were also sectioned into 1 or 4 cm sections and density and porosity was determined as described earlier.

3. RESULTS

Gravity and multiple corer data from stations GeoB 3703 and GeoB 3714 are shown in Figure 2 and Figure 3, respectively. However, as up to 15 cm or more of the surface sediment was disturbed from gravity coring, observations from the upper 20 cm of the GC should be interpreted with caution.

3.1. Sediment Description, Density, Porosity, and Organic Carbon

Sub-sampling the GC revealed a very heterogeneous sediment at both stations and several of the sub-sections were difficult to sub-core due to pocket-like sediment structures with an obvious higher water content. This sediment heterogeneity is strongly reflected in the scattered observations of both densities and porosities (Fig. 2a,b, 3a,b). In general, densities decreased from a maximum of approx. 1.3 g cm^{-3} immediately below the sediment surface to about 1.1 g cm^{-3} at the bottom of the sulfate zone at depths of 4 m (GeoB 3703) and 6 m (GeoB 3710), respectively. Below these depths densities increased to approx. 1.2 g cm^{-3} at 9 m depth on GeoB 3703 and 1.4 g cm^{-3}

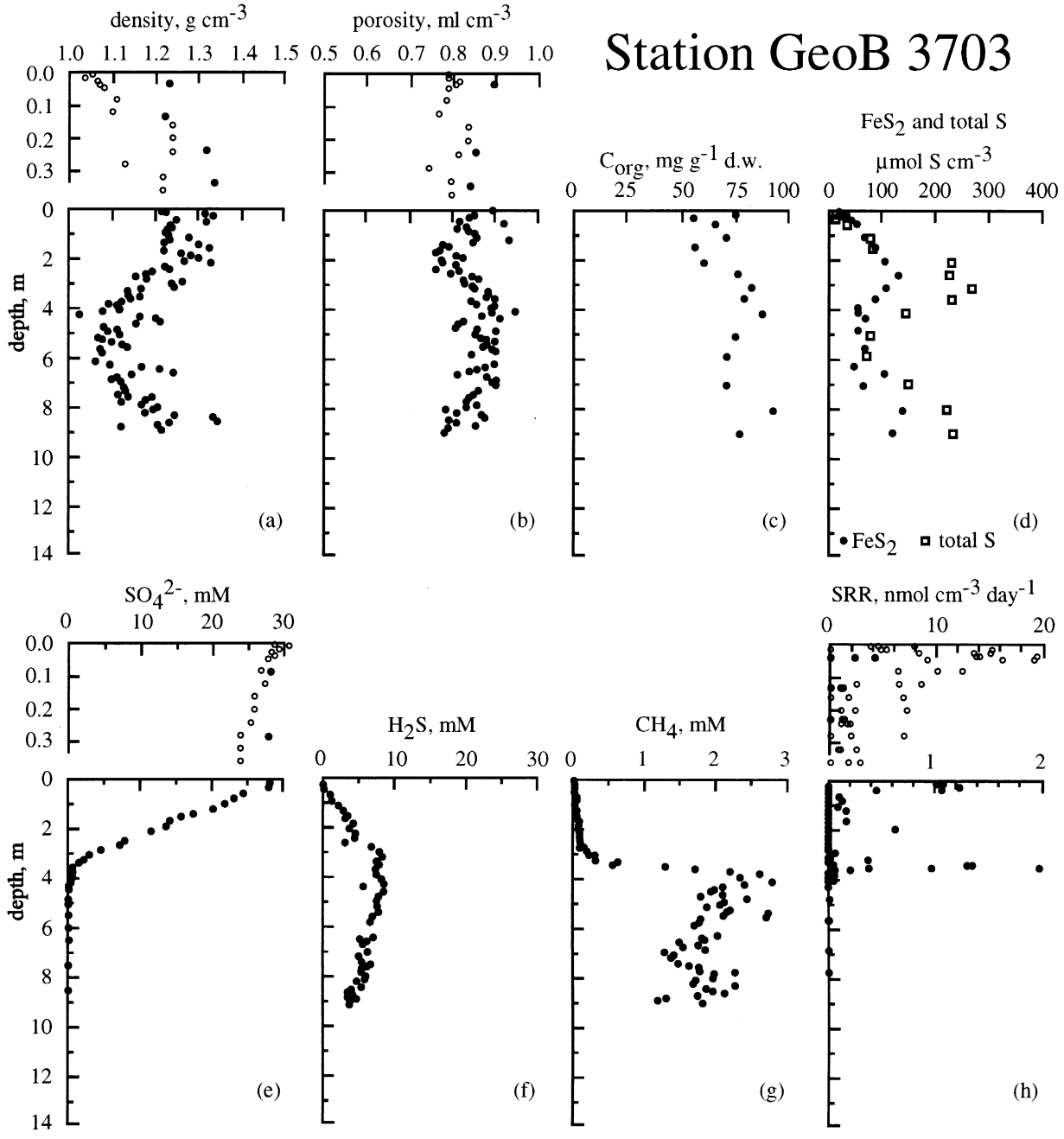

Fig. 2. Sediment data from Station GeoB 3703. Gravity core data (lower panel) are shown on a depth scale from 0 to 14 m whereas observations from the MuC (i.e., density, porosity, sulfate concentration, and sulfate reduction rate) are presented on a 0–30 cm depth scale (upper panel). Data from the upper 30 cm of the GC sampled sediment are also shown by solid symbols on the "MuC-figure". Note the changed rate-scale between the upper and lower panel on (h): SRR.

at about 12 m on GeoB 3714. At GeoB 3703 there was no overall change in porosity from the surface sediment to the bottom of the GC cores and an average porosity of 0.85 ± 0.04 ml cm^{-3} (n = 81) was calculated (Fig. 2b). A decrease in porosity from 0.87 ± 0.03 ml cm^{-3} (n = 5) at the surface to 0.75 ± 0.04 ml cm^{-3} (n = 57) at the bottom of the GC was observed at GeoB 3714 (Fig. 3b).

The organic carbon (C_{org}) content was high in the surface sediment at both stations (Fig. 2c and 3c) with surface concentrations of approx. 75 mg C_{org} g^{-1} dry weight and 37 mg C_{org} g^{-1} d.w. at GeoB 3703 and GeoB 3714, respectively. At GeoB 3703 C_{org} concentrations remained roughly constant with depth at approximately 73 mg C_{org} g^{-1} d.w. The organic content at GeoB 3714 decreased with depth to an average concentration of 24 ± 2 mg C_{org} g^{-1} d.w (n = 21) below 4 m. The carbon-nitrogen ratio at GeoB 3714 were 11.9 near the sediment surface and remained close to 12 with increasing sediment depth. At GeoB 3703, C/N ratios were also near 12 at the

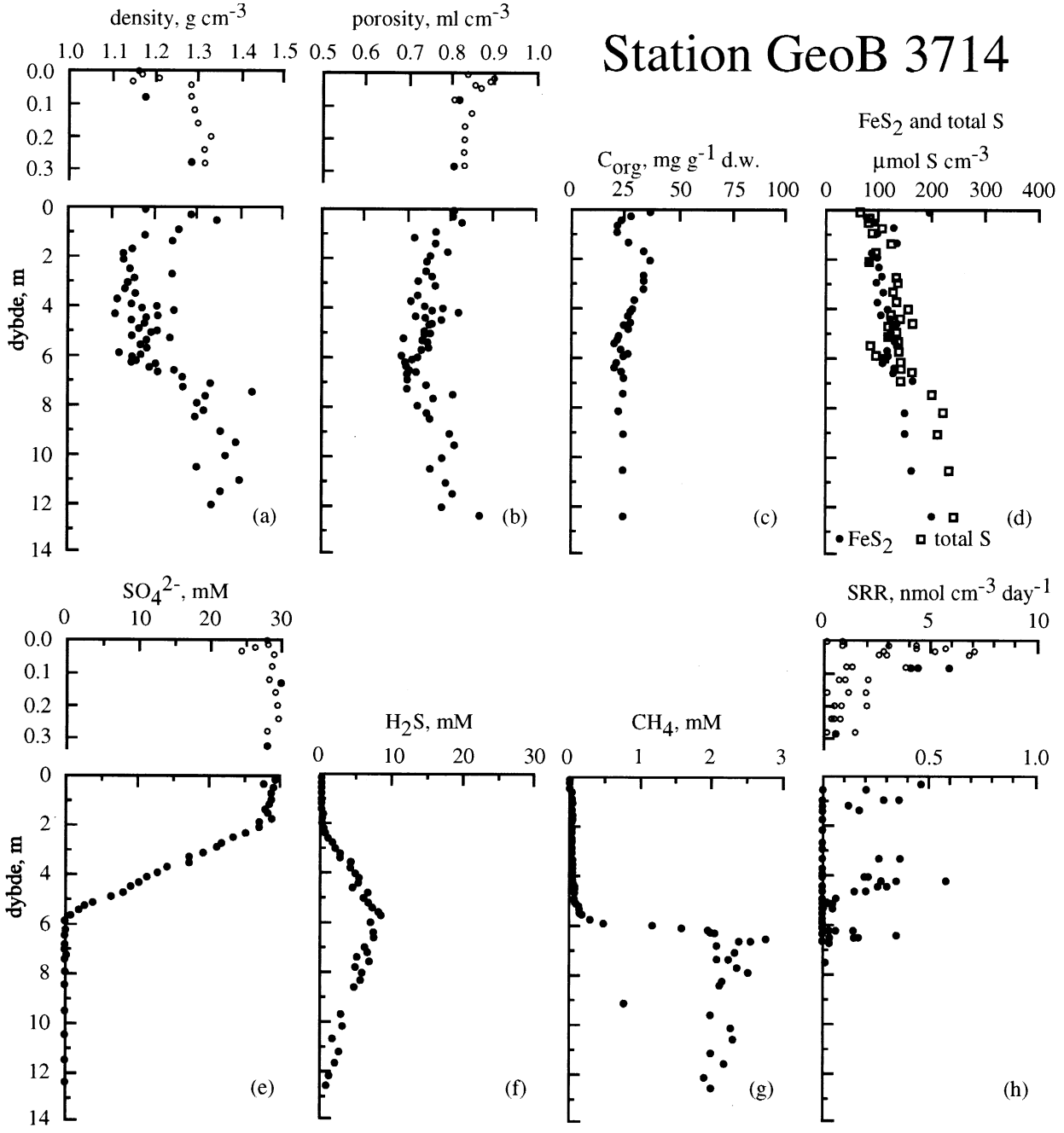

Fig. 3. Sediment data from Station GeoB 3714. Note the changed rate-scale between the upper and lower panel on (h): SRR. (For further details see also caption for Fig. 2).

surface but then increased to an average value of 15 with increased sediment depth (C/N-data not shown).

3.2. Solid Phase Sulfur

Iron monosulfide (FeS) concentrations were less than 2 μmol cm^{-3} throughout both cores and concentrations of S^o were <1 μmol cm^{-3} (data not shown). Pyrite sulfur at GeoB 3703 increased with depth from about 20 μmol cm^{-3} at the top of the GC to 105 μmol cm^{-3} at 265 cm depth (Fig. 2d). Below this depth, however, FeS_2 decreased over the next 140 cm to 55 μmol S cm^{-3} followed by a concentration increase to about 130 μmol S cm^{-3} at 900 cm depth. At two depth horizons on the station total sulfur exceeded the pyrite sulfur concentration: in the depth of 2.0–4.5 m by up to 160 μmol cm^{-3} and below 7 m by up to 110 μmol cm^{-3} (Fig. 2d). We attribute this difference to organic sulfur. Opposite to GeoB 3703, pyrite concentration on GeoB 3714 increased during the whole length of the gravity core; i.e., from about 80 μmol S cm^{-3} to 200 μmol S cm^{-3} at 13 m depth (Fig. 3d). Total sulfur equaled the concentration of pyrite sulfur in the upper 7 m of the sediment.

Below this depth, total sulfur exceeded pyrite by up to 75 μmol cm^{-3}.

3.3. Pore Water Concentrations of SO_4^{2-}, H_2S and CH_4

Sulfate concentrations were at sea water concentration at the sediment surface on both stations. At GeoB 3703 a linear depletion in SO_4^{2-} concentration was observed from 28.2 mM at the surface to 2.7 mM at a depth of 300 cm (Fig. 2e). At about 300 cm the sulfate gradient began to curve, indicating a net sulfate consumption around this depth. No SO_4^{2-} (i.e., <40 μM) was detected below 450 cm. At GeoB 3714 only an insignificant SO_4^{2-} depletion was observed in the upper 2 m of the sediment (Fig. 3e). Below this depth, however, SO_4^{2-} concentration decreased almost linearly with the most pronounced change in the SO_4^{2-} gradient between 550 cm (2.0 mM) and 600 cm. At depths below 700 cm was SO_4^{2-} not detected, i.e., <70 μM.

Total dissolved sulfide (H_2S) was detected on both stations from the top of the SO_4^{2-} depletion zone, i.e., near the sediment surface at GeoB 3703 and at approx. 2 m depth at GeoB 3714 (Fig. 2f and 3f). In the bottom of the SO_4^{2-} zone, H_2S reached a maximum value of approx. 8.5 mM at both stations. Below these depths H_2S concentration decreased but was, however, still detectable in the bottom of both GC cores.

Methane was detected throughout the sediment but in the upper part of the SO_4^{2-} zone in very low concentrations (<100 μM). At the bottom of this zone, however, a steep increase in CH_4 was observed immediately before the SO_4^{2-} pool became completely exhausted. At this depth, (here defined as the sulfate-methane transition zone; SMT) CH_4 increased within a few meters from <100 μM and up several mM (Fig. 2g and 3g). Due to the pressure release by bringing the sediment cores on deck, CH_4 degassed from the sediment at depths where the in situ CH_4 concentration exceeded atmospheric saturation, creating the scattered CH_4 concentration profile observed below the SO_4^{2-} zone. Of course, the loss of CH_4 from the deep CH_4 zone (>66% of in situ content at GeoB 3714) led to a dramatic change in the CH_4 concentration profiles at both stations, however, only at depths where in situ CH_4 partial pressure exceeded 1 atm.

Hence, even after a few days of storage it was possible to obtain realistic CH_4 concentrations in the SMT at depths where the in situ CH_4 concentration did not exceed the saturation concentration of 1.7 mM CH_4 at 1 atm, 4°C and 26‰ salinity, as calculated from Yamamoto et al. (1976).

3.4. Sulfate Reduction Rates

Bacterial sulfate reduction was observed on both stations, particularly in the surface sediment (Fig. 2h and 3h). The sulfate reduction rates were highest at GeoB 3703, with peak rates of up to almost 20 nmol cm^{-3} day^{-1} at 3–4 cm depth and exponentially decreasing with depth. Except for a few scattered observations below 30 cm, major SR was only observed in the SMT (at about 350 cm depth) with rates of up to 2 nmol cm^{-3} day^{-1}. At GeoB 3714 SRR of up to 7 nmol cm^{-3} day^{-1} were observed at 3–5 cm depth, declining with depth. In the SMT, SRR up to 330 pmol cm^{-3} day^{-1} were observed at about 645 cm depth. However, in contrast to GeoB 3703, a significant SR on GeoB 3714 was also observed between the surface sediment and the SMT. Here, between 330 cm and 500 cm, SRR were observed which were equivalent to or even exceeding the SRR in the SMT.

We had expected to be able to estimate the SRR based on a linear increase in $^{35}S_{red}$ after 24, 48 and 72 hours of incubation and this way to delimit the interference from the carry over of non-reduced ^{35}S to the reduced pool of sulfur (i.e., the blank value b, see Eqn. 1). However, a linear relationship between incubation length and sulfate reduced could unfortunately not be established at any of the two stations due to very heterogeneous sediments (see Discussion). Therefore, three independent SRR were calculated for each depth interval taking the blank value into account. At depth where the observed SRR $<$ SRR_{lim} (see Eqn. 2) the SRR was pictured as zero (Fig. 2h and 3h).

3.5. SRR Calculations Based on Direct Measurements ($^{35}SO_4^{2-}$ Labeling)

The $^{35}SO_4^{2-}$ labeling allowed us to calculate the SRR in different sediment zones and by summing up these contributions over the length of the entire SO_4^{2-} zone to estimate an areal sulfate reduction rate (SRR_{area}, μmol m^{-2} day^{-1}). At each depth three SRR were observed based on the three different incubation lengths (24, 48, and 72 hours, respectively, see Fig. 2f and 3f). Of the three SRR-values the highest and lowest represented the maximum and minimum SRR at this particular depth (i.e., SRR_{max} and SRR_{min}, respectively) whereas the middle value was the median SRR (i.e., SRR_{median}). The minimum and maximum SSR_{area} were calculated when respectively SRR_{min} and SRR_{max} at each depth were summed. The median SSR_{area} was calculated using the SRR_{median} from each particular depth interval. The depth dependent cumulated SSR_{area} determined from the $^{35}SO_4^{2-}$ labeling are shown in % of the total SSR_{area} on Figure 4 and in Table 1.

3.6. SRR Calculations Based on Sulfate Profile Interpretation (Mathematical Modeling)

Using the profile interpretation procedure of Berg et al. (1998) and the measured concentration profiles of SO_4^{2-} (CH_4 and H_2S) from the gravity cores as input, production (or consumption) rates were calculated as a function of depth. In short, this numerical procedure calculates a series of fits of one measured concentration profile at a time, and chooses the best fit based on an objective statistical comparison of the fits. With a chosen fit, the production profile is also known through the unique relation between concentration and production (Eqn. 3), which assumes steady-state conditions and accounts for the effects of molecular diffusion and irrigation (i.e., the pumping activity of tube-dwelling animals) or a similar transport mechanism that can be described as a non-local transport:

$$\frac{d}{dx}\left(\varphi D_s \frac{dC}{dx}\right) + \varphi\,\alpha\,(C_0 - C) + R = 0 \qquad (3)$$

where C is the pore water concentration, C_0 is the bottom water concentration, x is the depth, φ is the porosity, D_s is the sediment diffusivity, α is the irrigation coefficient, and R is the

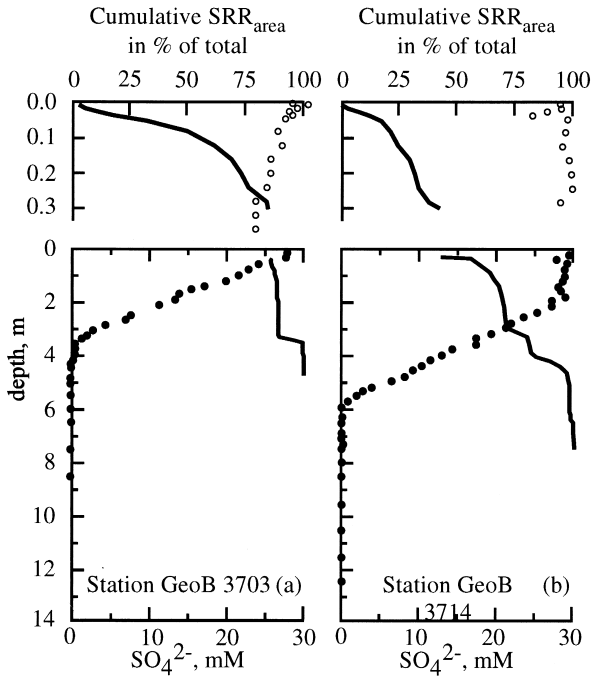

Fig. 4. Sulfate concentrations (open symbols: MuC-cores and closed symbols: GC-cores) and cumulated areal sulfate reduction rate (SRR_{area}) in % of total SRR_{area} (solid line) calculated from $^{35}SO_4^{2-}$ direct measurements at (a) Station GeoB 3707 and (b) Station GeoB 3714. The upper and lower panels show observations from the MuC and GC, respectively. Note that the cumulated SRR_{area} starts at 30 cm in the GC.

net rate of production (or consumption if R is negative). Although irrigation is a complex transport phenomenon and is three-dimensional by nature (Aller 1980), it is widely recognized that irrigation can be include in one-dimensional formulations as in Eqn. 3, by using the non-local source-sink function suggested by Boudreau (1984). In the profile interpretation procedure, the production profile (R) is assumed to consist of a number of depth intervals each with a constant production or consumption rate (for further details see Berg et al. 1998).

In our calculations, we used linear fits of porosities for both stations: At GeoB 3703 a linear fit through all measured porosities gave a depth independent value of 0.85 ± 0.04 ml cm^{-3} (n = 81) and at GeoB 3714 a depth dependent fit was observed of $0.74 + 0.17 \cdot 10^{-4}$ x ± 0.04 ml cm^{-3} (n = 57) where x is the depth in cm. D_s was calculated as $D/(1+3(1-\varphi))$ where D is the diffusivity in water (Iversen and Jørgensen, 1993). In the first series of interpretations irrigation was neglected ($\alpha = 0$) which resulted in the production profiles shown in Figure 5 and Figure 6. While all calculated concentration profiles fit the measured data well, the best fits were obtained for SO_4^{2-} for both stations with R^2 values as high as 0.998 and 0.997 for GeoB 3703 and GeoB 3714, respectively.

4. DISCUSSION

The sulfate reduction rates measured by $^{35}SO_4^{2-}$ labeling unequivocally demonstrate that SR proceeds not just within the SMT, but also in the overlying SO_4^{2-} zone (Fig. 2h and 3h). In fact, the major fraction of SRR_{area} in the upwelling area of the Namibian shelf took place in the upper 30 cm of the surface sediment with 83% of the total SRR_{area} at GeoB 3703 and 34–38% at GeoB 3714 (Table 1).

In sharp contrast to the SRR measured by $^{35}SO_4^{2-}$ labeling are the rates calculated from SO_4^{2-} profile interpretations assuming that all transport takes place by diffusion. These modeled SRR show that sulfate reduction only proceeds in the SMT (Fig. 5a and 6a), consistent with the conclusions of Niewöhner et al. (1998). Here it is worth distinguishing between rates of net sulfate consumption and gross sulfate reduction. Both the gradient modeling approach of Niewöhner et al. (1998) and the curve fitting approach applied here provide information only on the net sulfate consumption rates. Total rates of organic matter mineralization via SR may be seriously underestimated by only examining the net sulfate consumption rates. In the two cores presented here, the modeled SRR_{area}, or areal rates of net sulfate consumption, underestimate by 89% at GeoB 3703 ((2221–237)/2221) and by 86% at GeoB 3714 the (gross) SRR as measured by the $^{35}SO_4^{2-}$ labeling method. Thus, earlier studies where SRR have been calculated by Fick's First Law, Flux = $-\varphi D_s$ dC/dx, should be interpreted with care (e.g., Skyring, 1987; Canfield 1991) as they principally reflect areal rates of net sulfate consumption. Hence, the gross SRR_{area} has most likely been underestimated. At some of these sites the modeled SRR based on SO_4^{2-} gradients may even be a better

Table 1. Areal sulfate reduction rates (SRR_{area}) calculated from $^{35}SO_4^{2-}$ direct measurements. Expected rates at Station GeoB 3714 are shown in brackets (see discussion).

	Station GeoB 3703				Station GeoB 3714					
	Depth cm	μmol m^{-2} day^{-1} Range	Median	SRR_{area} % of total[b]	Depth cm	μmol m^{-2} day^{-1} Range	Median		SRR_{area} % of total[b]	
	0–30	1067–2277	1852	83%	0–30	301–756	425		38%	(34%)
					30–200	39–546	340		30%	(27%)
	30–250	0–379	118	6%	200–505	53–597	327		29%	(26%)
SMT[a]	250–450	47–437	251	11%	505–700	5–84	29[c]	(159)	3%[c]	(13%)
total	0–450	1114–3493	2221	100%	0–700	398–1983	1121	(1251)	100%	(100%)

[a] Sulfate-methane transition zone.
[b] Calculated from median value.
[c] Probably underestimated (see text).

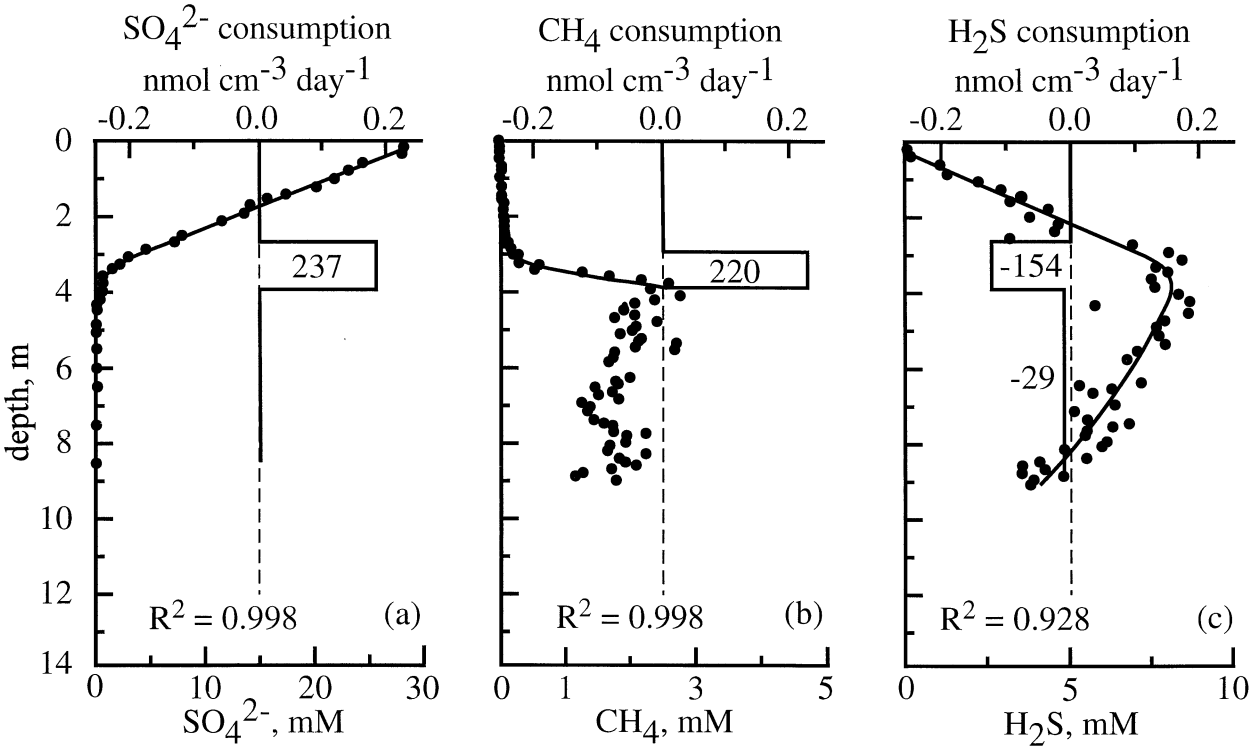

Fig. 5. Station GeoB 3703. Best fitted concentration profiles and modeled rates of consumption (neglecting irrigation) of (a) SO_4^{2-}, (b) CH_4, and (c) H_2S. Areal rates are shown in μmol m^{-2} day^{-1}, negative rates mean production.

measure of deep methane flux rather than organic carbon decomposition coupled directly to SR.

4.1. Sulfate Reduction Above the Sulfate-Methane Transition Zone

In both cores SRR were highest at the surface and then exponentially decreased with depth. At depths greater than 30 cm the occurrences of measurable SRR tended to be sporadic and was probably associated with distinct high reactivity environments. These observations suggest that both sulfate reducing bacteria and sulfate reduction activity was present in varying degrees throughout the entire SO_4^{2-} zone in the sediments studied. Similar observations have also been made at other locations e.g. the upwelling site on the Peru Margin (Fossing, 1990; Parkes et al., 1993) and Danish waters, Aarhus Bay (Thode-Andersen and Jørgensen, 1989) and Kattegat (Iversen and Jørgensen, 1985).

The two sediment cores in this study can in no way be thought of as a series of uniformly deposited homogenous layers. Rather the sediment was, at the centimeter scale, a mixture of various sediment types, porosities, pockets of fecal pellets, and both open and filled-in tubes. At the sub-millimeter scale the sediment consisted of compacted areas of nannofossil or diatomaceous ooze, fecal pellets, pyritized foraminifera and tube-porewater interfaces. The heterogeneity of the sediment became obvious already during sub-sampling and was later documented both from the "noisy" density and porosity gradients (Figs. 2a,b, 3a,b) and the non-linearity between incubation length vs. sulfate reduced. Particularly at GeoB 3714 we observed, at most depths, tubular patches of (light) gray sediment (up to 15 mm (ID) or even thicker) mixed into in the bulk grayish-brown sediment. The gray sediment was much more difficult to sub-sample, due to what appeared to be a higher content of pore water. In a few sections we were even able to follow some of these tubular gray patches through the sediment for a few centimeters before they slanted out through the side of the core.

In spite of the large degree of variability in the deeper core data, it is clear from Figures 2h and 3h that measurable and significant amounts of SR took place within the zone of the steep (but not changing) SO_4^{2-} gradient at both stations. Sulfate reduction was particularly pronounced at GeoB 3714 where 53–597 μmol SO_4^{2-} m^{-2} day^{-1} was reduced between 200 cm and 505 cm (Table 1, Fig. 3h and 4b). This accounted for about 29% of the observed total SRR_{area} at GeoB 3714. However, there is no evidence from the organic carbon contents, from the C/N ratios, nor from the core stratigraphy (Schulz et al., 1996) that this would be a particularly reactive layer. The sediments lying between approx. 300 and 700 cm are thought to represent a deglaciation phase between the last glacial period and the Holocene (Schneider et al., 1992). Average sedimentation rates for the deglaciation are 110 cm ka^{-1} as compared to 30 cm ka^{-1} both for the deeper glacial sediments and the overlying Holocene sediments (Schneider et al., 1992). The relatively high SRR may, therefore, reflect a component of reactive material that was rapidly buried and is still being slowly consumed via SR.

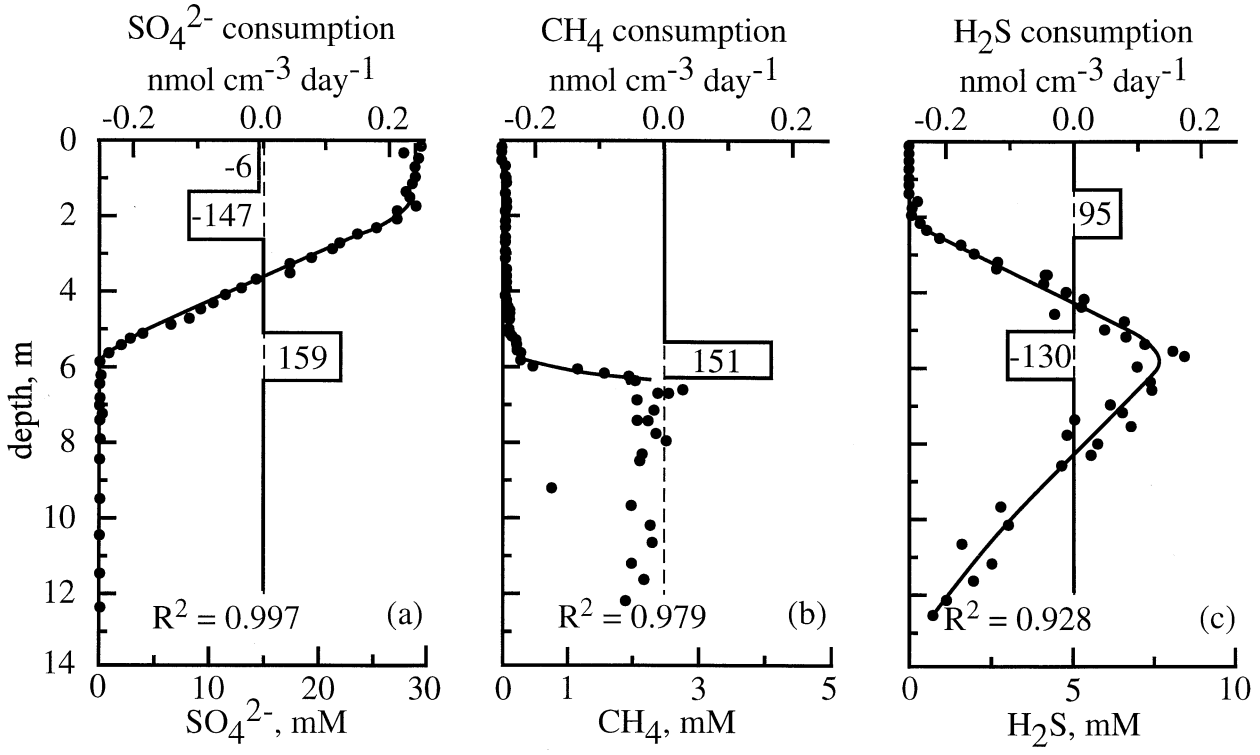

Fig. 6. Station GeoB 3714. Best fitted concentration profiles and modeled rates of consumption (neglecting irrigation) of (a) SO_4^{2-}, (b) CH_4, and (c) H_2S. Areal rates are shown in μmol m^{-2} day^{-1}, negative rates mean production.

4.2. The Sulfate-Methane Transition Zone (SMT)

Only in the SMT a net production of H_2S was noticed (Fig. 5c and 6c). There was, anyhow, at both stations an imbalance between the rates of SR and sulfide production; (237−154−29 =) 54 μmol m^{-2} day^{-1} at GeoB 3703 (Fig. 5) and 29 μmol m^{-2} day^{-1} at GeoB 3714 (Fig. 6). We explain this discrepancy from sulfide precipitation with iron or incorporation of H_2S into organic compounds. Thus, according to this (54/237) 23% and 18% of the produced H_2S, (at GeoB 3703 and GeoB 3714, respectively) precipitated in the sediment. This was further supported from the observed increase in both FeS_2 and organic sulfur with depth (Fig. 2d and 3d). At GeoB 3714 most of the sulfide precipitated as pyrite whereas a larger sulfide fraction was observed as organic sulfur at GeoB 3703. This suggests that the organic matter at GeoB 3703, the more productive station, consists of more reactive (towards sulfide) organic compounds than GeoB 3714.

Consistent with the findings of Niewöhner et al. (1998), the modeled downward SO_4^{2-} flux into the SMT at both stations was perfectly balanced by the upward CH_4 flux (Fig. 5a,b and 6a,b). Furthermore, at GeoB 3703 we observed an excellent agreement between the modeled SRR and the rates measured by the $^{35}SO_4^{2-}$ labeling (Fig. 5a and Table 2). At GeoB 3714, however, we observed a large discrepancy between the measured SRR of 5–84 μmol m^{-2} day^{-1} (Table 1) and the modeled rate of 159 μmol m^{-2} day^{-1} (Fig. 6a). Most likely this discrepancy might be explained from the way the 1297 cm long sediment core was cut into 13 one meter sections. Not knowing prior to sectioning at what depth the SMT was located, the core was unfortunately cut at 587 cm. This cut appears to have been placed in the middle of the SMT (Bloch, 1986) as determined from the sulfate profile interpretation procedure (see Fig. 6a). Thus, the SMT was more or less split between two 1 m subsections. Since the top 5 cm of the lower section (587–592 cm) was discharged as described previously and the bottom 6 cm (581–587 cm) of the above GC-section also was not sampled, 11 cm (or about 10%) of the "more important part" of the SMT was unfortunately lost. Therefore, a possible increased SRR in this section did not contribute to the overall measured SRR_{area} in the SMT. We therefore argue, that in this zone the measured SRR was most probably underestimated by at least 47% (i.e., (159−84)/159). Thus, rather than 3% of the total SRR_{area} taking place in the SMT (Table 1) more likely (159/1251 =) 13% of the overall SRR_{area} proceed in this zone, the same fraction as observed at GeoB 3703. Fractions of similar sizes have also been observed in the SMT at other locations where SRR have been measured by $^{35}SO_4^{2-}$ injections throughout the entire SO_4^{2-} zone (Iversen and Jørgensen, 1985; Thode-Andersen and Jørgensen, 1989; Hansen et al., 1998).

Our observations show that most of the sulfate reduction proceeds above the SMT and confirm that SR in the SMT was fueled entirely by the upward flux of CH_4. From the near perfect 1:1 stoichiometry between SO_4^{2-} and CH_4 consumption observed in the SMT it is tempting to argue that CH_4 was oxidized by sulfate reducing bacteria as such conclusions often have been drawn from similar observations (Martens and Berner, 1977; Alperin and Reeburgh, 1985; Iversen and Jørgensen, 1985). However, it should be noticed that from the

Table 2. Measured and modeled SRR_{area} integrated over the length of the gravity core using depth intervals predicted by the profile interpretation procedure. Irrigation values (α) are calculated according to Eqn. 6 (see text).

	Measured SRR μmol m^{-2} day^{-1}		Modeled SRR μmol m^{-2} day^{-1}		
Depth cm			Diffusion only	Diffusion and irrigation	Irrigation value (α) $year^{-1}$
Station GeoB 3703					
8–137	1065		0	1127	0,073
137–265	17		0	35	0,000
265–394	239		237	239	0,000
394–450	10		0	1	0,000
8–450	1331		237	1402	
Station GeoB 3714					
13–138	477		−6	546	0,270
138–263	39		−147	86	0,032
263–388	125		0	167	0,004
388–513	189		0	167	0,004
513–639	12	(159)[a]	159	168	0,000
639–700	15		0	0	0,000
13–700	857	(1004)[a]	6	1134	

[a] Expected SRR (see text).

scientific literature it has not been possible to confirm such a direct coupling between methane oxidation and sulfate reduction, as all attempts to isolate a methane oxidizing, sulfate reducing bacterium, to our knowledge, have failed. For the same reasons it has therefore been proposed that CH_4 is not oxidized by a sulfate reducing bacteria but instead through a consortium of two or more bacteria species, including a sulfate reducer (Hoehler et al., 1994; Hansen et al., 1998). According to this theory CH_4 is oxidized to hydrogen and bicarbonate by "reverse methanogenesis" followed by H_2 consumption through SR. This way H_2 concentration is kept low and "reverse methanogenesis" becomes an energetically favorable process (exergonic) and the observed 1:1 stoichiometry is ultimately retained. This theory would appear to fit with our observations. In the SMT sulfate reduction took place over several centimeters of the CH_4 gradient and not only at the exact break in the CH_4 curve (where CH_4 concentrations are very low). Within the gradient the CH_4 concentration was much higher than at the break and the concentrations of H_2 was expected to be low. Hence, assuming that sulfate reducing bacteria present in the SMT have a high affinity for both SO_4^{2-} and H_2, methane oxidation by "reverse methanogenesis" should be favorable over the depths of the steep CH_4 gradient, until SO_4^{2-} is absolutely exhausted.

4.3. Another Transport Mechanism in Addition to Molecular Diffusion?

In the SMT we were able to verify the measured SRR from modeled fluxes of SO_4^{2-} and CH_4. However, far more puzzling, and thus challenging, was it to find verification for the measured SRR above the SMT which did not agree with SRR from the profile interpretations (Table 2). Here, in the top ca. 2 m of GeoB 3714 we observed the most significant SRR_{area} despite no change in the overall SO_4^{2-} concentration and also below two meter the SO_4^{2-} gradient remained essentially flat despite observations of SR. Similar observations were done at GeoB 3703 over the linear SO_4^{2-} concentration decrease (Table 2). It is important to note that the modeled SRR_{area} were all done assuming that transport takes place only by molecular diffusion (i.e., Eqn. 3 ignoring irrigation ($\alpha = 0$)) but anyhow based on the excellent fits of the SO_4^{2-} concentration profiles. Above the SMT at both stations the modeled SRR did not reveal any SR and at GeoB 3714 modeling even showed a net SO_4^{2-} production (negative SRR value, see Table 2 and Fig. 6a) despite that SR was measured (Fig. 3h).

We argue that the $^{35}SO_4^{2-}$ measurements return the true SRR and, as a consequence, that a highly active transport mechanism other than molecular diffusion is supplying the deeper sediment layers with SO_4^{2-} to maintain the significant SR we measured. Based on our observations of tubes and burrows in the sediments, the most obvious transport mechanism is a non-local transport of PW solutes, like irrigation, which bypass major parts of the sediment matrix through the tubes and burrows. Several studies have shown that irrigation can contribute significantly to the overall transport of solutes in sediments, and in some situations may be the dominant transport mechanism (Aller, 1983; Pelegri et al., 1994; Wang and van Cappellen, 1996).

Irrigation, as a transport mechanism, is generally used to designate PW movement in tubes or burrows caused by the pumping activity or movement of tube-dwelling animals (Boudreau, 1997). While processing the sediment onboard the ship, we did observe thumb-thick, 2 cm (ID) "tube-like" structures filled with sediment. These "tubes" sloped into the sediment from the side of the core, twisting their way more or less vertically through the sediment before they slanted out of the sediment core some centimeters below their entrance. Most probably these "tubes" should be interpreted as relict burrows.

Smaller tubes up to 8 mm (ID) but without sediment fillings were also observed in some of the sediment sections at depths down to 6 meters. Also these tubes ran hither and thither through the sediment and therefore we were not able to confirm their connection to the sediment surface. Back in the laboratory we carefully broke open some of the sediment sections along the tubes. On fracture surfaces we were able to study the inside tube walls under a dissection microscope and we observed distinct fecal pellets at all depths which indeed confirmed that the open tubes were or had been inhabited by animals.

Hypothesizing that tube-dwelling animals are present in the sediment, we have investigated if their pumping activities can transport the necessary amount of SO_4^{2-} down into the sediment to explain the measured SRR and the observed SO_4^{2-} profiles. We have done this by using the results form the first SO_4^{2-} profile interpretations where irrigation was neglected ($\alpha = 0$) allowing Eqn. 3 to be expressed as

$$\frac{d}{dx}\left(\varphi D_s \frac{dC}{dx}\right) = SRR_{\text{diffusion only}} \quad (4)$$

The equation that accounts for both the effects of molecular diffusion and irrigation, and gives the measured SRR can be expressed as (from Eqn. 3)

$$\frac{d}{dx}\left(\varphi D_s \frac{dC}{dx}\right) + \varphi \alpha (C_0 - C) - SRR_{\text{measured}} = 0 \quad (5)$$

Note that the values of $SRR_{\text{diffusion only}}$ and SRR_{measured} are known and listed in Table 2. Assuming that the diffusive transport (represented by the first term in both Eqn. 4 and 5) is exactly the same whether irrigation is included or not, Eqn. 4 and 5 can be combined to yield

$$\alpha = \frac{SRR_{\text{measured}} - SRR_{\text{diffusion only}}}{\varphi (C_0 - C)} \quad (6)$$

The irrigation values, α (defined by Boudreau (1984) as fraction exchanged per unit time) were calculated from the values of $SRR_{\text{diffusion only}}$ and SRR_{measured} given in Table 2 and values of *C* found in the first interpretation of the two SO_4^{2-} profiles. As a control, these α values (Fig. 7a and Fig. 8a) were used in two new profile interpretations of the SO_4^{2-} profiles which gave an excellent agreement between the measured and the calculated SRR (Fig. 7b and 8b, Table 2).

Boudreau (1997) has reviewed values of α in the range from 0 to 300 $year^{-1}$ and found typically the highest values for shallower water systems, and typically decreasing with sediment depth, which is intuitively expected. The only α value we have found that is valid for water depths comparable to our stations was given by Christensen et al. (1987) who reported α to be approximately 2 $year^{-1}$ for a site at 1800 m depth. Based on these studies, we believe our α values are realistic not only with respect to their actual numeric value, but also to the variation with depth.

In our estimates of α we assumed that all transport takes place by molecular diffusion and irrigation. Other transport mechanisms, like bioturbation (i.e., the diffusion-like transport caused by random movements of fauna) and burial of SO_4^{2-} rich bottom water as part of the ongoing sedimentation, are also active in the sediment. We have evaluated their importance.

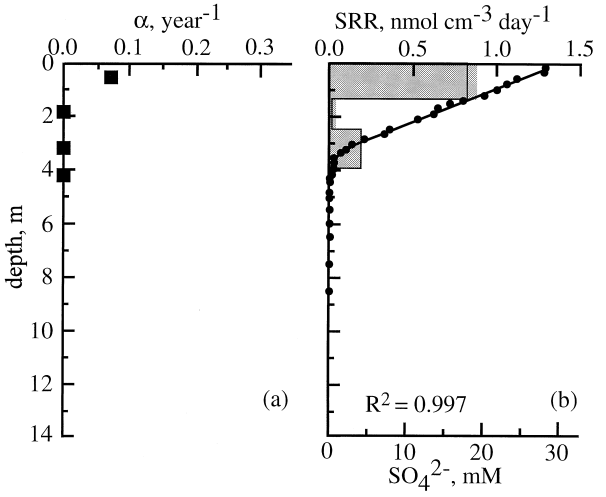

Fig. 7. Stations GeoB 3703. (a) Irrigation values, α, and (b) SO_4^{2-} concentration and SRR over the length of the gravity core. Depth intervals were predicted by the profile interpretation procedure (see text). Modeled SRR are shown as solid bars and SRR measured by $^{35}SO_4^{2-}$ labeling as open bars (i.e., a thin line). Notice that the two sets of bars are almost identical.

Since bioturbation is commonly described as a diffusive process (Boudreau 1997) where the intensity is expressed through the biodiffusivity (D_B), the effects of bioturbation vs. molecular diffusion are directly reflected in the ratio between D_B and the sediment diffusivity (D_s) (see Eqn. 3). D_s was calculated in the profile interpretation procedure and a representative mean value for our sites equals 3.4 10^{-6} cm^2 s^{-1}. The regression for D_B in the top layer of sediments ($\sim$ few cm) vs. water depth suggested by Middelburg et al. (1997) gives an average D_B value of 0.17 10^{-6} cm^2 s^{-1} for the two sites. The low ratio

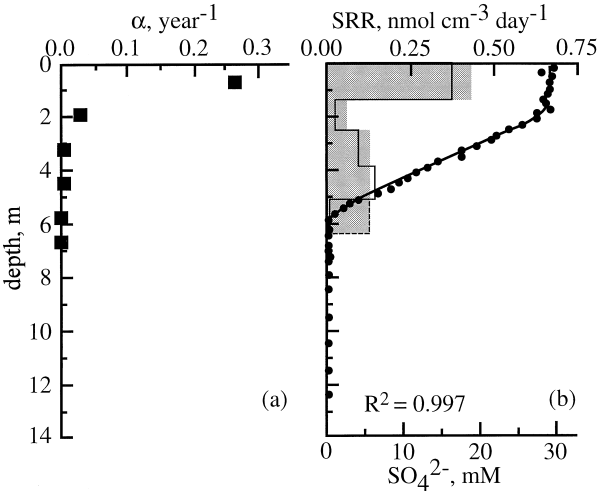

Fig. 8. Stations GeoB 3714. (a) Irrigation values, α, and (b) SO_4^{2-} concentration and SRR over the length of the gravity core. Depth intervals were predicted by the profile interpretation procedure (see text). Modeled SRR are shown as solid bars and SRR measured by $^{35}SO_4^{2-}$ labeling as open bars (i.e., a thin line). The broken line at 513–639 cm shows the expected SRR (see text). Notice that the two sets of bars are close to identical.

between D_B and D_s (0.05), and also the fact that D_B decreases strongly with sediment depth (Boudreau 1997) and often is assumed to equal zero at sediment depths of 10 to 30 cm, justify our exclusion of bioturbation in our calculations. If we assume similar burial rates for PW and solid sediment we can express the burial flux of SO_4^{2-} rich bottom water over the sediment surface as $\varphi w C_0$ where w is the sedimentation rate and C_0 is the bottom water concentration of SO_4^{2-}. With an average porosity of 0.8 for the two sites, an average sedimentation rate of approximately 0.05 cm $year^{-1}$ (Schneider et al., 1992), and a bottom water concentration of 30 mM, this flux can be estimated to 33 μmol m^{-2} day^{-1}. Comparing this flux of SO_4^{2-} into the sediment with the modeled depth integrated SRR of 1402 and 1134 μmol m^{-2} day^{-1} (Table 2) shows that this transport of SO_4^{2-} by sedimentation is insignificant to the combined effect of molecular diffusion and irrigation.

The modeled SRR with and without irrigation that are given in Table 2 clearly show the important role that irrigation can have even with the relatively small α values that we have estimated. For both stations the depth integrated SRR calculated with irrigation included are many fold higher than the rates found when only molecular diffusion was taken into account. In other words, in our model irrigation was by far the dominant transport process supplying the deeper sediment layers with sufficient SO_4^{2-} for maintaining the measured SRR.

4.4. Tube Dwelling Animals at Meter's Depth in Deep Sea Sediments

Unfortunately we did not find *the* animal which would be a strong evidence of our proposed irrigation hypothesis. A simple calculation might explain why. A rough estimate using the expression for α derived by Boudreau (1984), shows that α values of about 0.1 $year^{-1}$ can be achieved from 10–15 actively irrigating animals per m^2 each habituating a 1 cm (ID) tube. If these animals were evenly distributed in the sediment the possibility of catching 1 animal in the gravity corer (113 cm^2) was 11–17 %. Thus to catch at least one animal with 95% possibility more than 25 gravity cores should be recovered.

Although reports on tubes and burrows that penetrate deep into sediments are sparse, such observations have also been made in deep sea sediments at other locations. Tubes and burrow-like structures between 0.5 mm and 5 mm (ID) penetrating >2 meters into the sediment were observed in the Atlantic at water depths of about 5000 m (Thomson and Wilson, 1980; Weaver and Schultheiss, 1983). Larger burrows of up to 3 cm (ID) reaching the bottom of a 45 cm deep box corer were observed in eastern equatorial Pacific (Berger et al., 1979) and also reported from the north-west African continental margin sediments (Wetzel, 1981). From North Pacific sediments Nickerson (1978) reported of (quoted from Thomson and Wilson, 1980): "open burrows of a few millimeters in diameter to depths of a meter or more". Like in our observations, Weaver and Schultheiss (1983) also observed filled burrows which were wider than their open equivalents (to quote Weaver and Schultheiss, 1983): "either due to materiel falling from the walls during the filling process or because the open burrows have partially closed during coring". All these reports on deep penetrating tubes and burrows have in common, that the animal(s) responsible for these structures was/ were not found and thus identified.

Only Romero-Wetzel (1987) has observed animals (a sipunculan of the genus, *Golfingia*, subgenus *Nephasoma*) at 30 cm depth habituating a <1 mm (ID) and 50 cm long tube at water depths between 1261 and 1969 m (Norwegian continental slope). However, the sipunculans could not construct the up to 8 mm (ID) open tubes observed in the sediments of this study, which (if partly collapsed during coring) could be even wider in situ as argued by Weaver and Schultheiss (1983). Thus, the discovery of the organism(s) responsible for the larger tubes and burrows in deep-sea sediments still awaits its disclosure.

Our SO_4^{2-} profile interpretations show that the measured SRR on both stations can be explained by the presence of a non local transport mechanism supplying the deeper sediment layers with SO_4^{2-} rich water from the above water column. As we have argued this transport can very well originate from tube-dwelling animals through their pumping activity, but we believe that a similar transport pattern can also be established in absence of such animals by ebullition of for example CH_4 gas escaping the sediment through old tubes or borrows. When a bubble of CH_4 gas leaves a given sediment layer and moves upward through a tube and into the overlying water column, a certain volume (the bubble plus a body of water that is pushed in front of the bubble) must be replaced. This results in a downward-directed transport of water which happens in other tubes that are more or less connected (through tubes or through the porous sediment matrix) to the tube in which the bubble is rising. To our knowledge this transport mechanism has not been proposed before for sediments as deep as in this study (~2–3 m). Further studies must be done to determine how effectively this transport mechanism can move bottom water down into these sediments. For sandy sediments and much smaller sediments depths (~0.3 m) O'Hara et al. (1995) have shown that ebullition of CH_4 gas can facilitate such a transport in the sediment matrix, and also that the this transport can contribute significantly to total vertical transport.

4.5. Implications

We conclude, by suggesting, that the extension of the SO_4^{2-} penetration depth through non-local exchange of pore waters and the presence of meter deep SR has an important influence on the pathways of organic matter mineralization in these continental slope sediments. Niewöhner et al. (1998) suggested that it is the upward CH_4-flux that drives SR in the SMT and hence, the SO_4^{2-} penetration depth. We wish to expand upon this idea and suggest that, while the net sulfate consumption is balanced by the upward CH_4 flux, deep pore water exchange due to irrigation allows for deeper penetration of the SO_4^{2-} and consequently controls the depth of formation of an expanded sulfate reduction zone.

Taking GeoB 3714 as a example, deep penetration of SO_4^{2-} allows for a greater residence time of organic carbon in the sulfate reduction zone. Thus, a greater fraction of organic carbon is consumed through bacterial sulfate reduction. It is interesting to note that although depth integrated sulfate reduction in the upper 20 cm of sediment is four-fold higher at GeoB 3703 than at GeoB 3714, the total SRR_{area} is only double. Less organic carbon reaching the methanogenic zone would also

expectedly result in a lower CH_4 flux, which would, as a positive feedback, reduce the consumption of SO_4^{2-} and lead to a greater sulfate penetration. Thus, the depth of SO_4^{2-} penetration plays an important role in regulating how much organic material may reach the methanogenic zone. For the continental margin sediments of the South-West coast of Africa, we conclude that deep, non-local exchange of pore waters is the principal process controlling this deep sulfate penetration and the pore water distribution of other species involved in early diagenesis.

Acknowledgments—We are indebted to Prof. H. D. Schulz who graciously assisted in making our participation in the Meteor Cruise 34/2 both possible and productive. We also gratefully acknowledge Captain Bruns, the crew aboard the R/V Meteor, and colleagues from the University of Bremen, in particular B. Donner and K. Dehning, who assisted us in obtaining and processing cores. Drs. S. Forster and W. Ziebis are thanked for their help in identifying burrows and fecal pellets. K. Neumann skillfully performed many of the analyses. Two anonymous reviewers are thanked for their critical comments which have improved the paper. This research was sponsored by the German Science Foundation (DFG) Special Research Project (SFB 261) at the University of Bremen, "The South Atlantic in the late Quaternary" and the Max-Planck-Society, Munich.

REFERENCES

Aller C. A. (1980) Quantifying solute distributions in the bioturbated zone of marine sediments by defining an average microenvironment. *Geochim. Cosmochim. Acta* **44,** 1955–1965.

Aller C. A. (1983) The importance of the diffusive permeability of animal burrow linings in determining marine sediment chemistry. *J. Marine Res.* **41,** 299–322.

Aller R. C., Blair N. E., Xia Q., and Rude P. D. (1996) Remineralization rates, recycling, and storage of carbon in Amazon shelf sediments. *Cont. Shelf Res.* **16,** 753–786.

Alperin M. J. and Reeburg W. S. (1985) Inhibition experiments on the anaerobic methane oxidation. *Appl. Environ. Microb.* **50,** 940–945.

Battersby N. S., Malcolm S. J., Brown C. M., and Stanley S. O. (1985) Sulphate reduction in oxic and sub-oxic North-East Atlantic sediments. *FEMS Microb. Ecol.* **31,** 225–228.

Berg P., Risgaard-Petersen N., and Rysgaard S. (1998) Interpretation of measured concentration profiles in the sediment porewater. *Limnol. Oceonog.* **43,** 1500–1510.

Berger W. H., Ekdale A. A., and Bryant P. P. (1979) Selective preservation of burrows in deep-sea carbonates. *Mar. Geolog.* **32,** 205–230.

Berner R. A. (1964) An idealized model of dissolved sulfate distribution in recent sediments. *Geochim. Cosmochim. Acta* **28,** 1497–1503.

Bianchi A. and Garcia J. (1993) In stratified waters the metabolic rate of deep-sea bacteria decreases with decompression. *Deep-Sea Res. I* **40,** 1703–1710.

Blair N. E. and Aller R. C. (1995) Anaerobic methane oxidation on the Amazon shelf. *Geochim. Cosmochim. Acta.* **59,** 3707–3715

Bloch A. (1986) *Murphy's Law and other reasons why things go wrong!* Sloan Publishers.

Boetius A., Ferdelman T., and Lochte K. (in press) Bacterial turnover of organic carbon in sediments of the deep Arabian Sea in relation to vertical flux. Deep Sea Research II.

Borowski W. S., Paull C. K., and Ussler III W. (1997) Carbon cycling within the upper methanogenic zone of continental rise sediments: An example from the methane-rich sediments overlying the Blake Ridge gas hydrate deposits. *Marine Chem.* **57,** 299–311.

Boudreau, B. P. (1984) On the equivalence of nonlocal and radial-diffusion models for porewater irrigation. *J. Marine Res.* **42,** 731–735.

Boudreau B. P. (1997) *Diagenetic Models and Their Implementation*. Springer-Verlag.

Burns S. J. (1998) Carbon isotopic evidence for coupled sulfate reduction-methane oxidation in Amazon Fan sediments. *Geochim. Cosmochim. Acta* **62,** 797–804.

Canfield D. E. (1991) Sulfate reduction in deep-sea sediments. *Am. J. Sci.* **291,** 177–188.

Christensen, J. P., Smethie, W. M., and Devol A. H. (1987) Benthic nutrient regeneration and denitrification on the Wasington continental shelf. *Deep-Sea Res.* **34,** 1027–1–47.

Cline J. D. (1969) Spectrophotometric determination of hydrogen sulfide in natural waters. *Limnol. Oceanog.* **14,** 454–458.

Devol A. H. and Christensen J. P. (1993) Benthic fluxes and nitrogen cycling in sediments of the continental margin of the eastern North Pacific. *J. Marine Res.* **51:** 345–372.

Devol A. H., Anderson J. J., Kuivila K., and Murray J. W. (1984) A model for coupled sulfate reduction and methane oxidation in sediments of Saanich Inlet. *Geochim. Cosmochim. Acta* **48,** 993–1004.

Edenborn H. M., Silverberg N., Mucci, A., and Sundby B. (1987) Sulfate reduction in deep coastal marine sediments. *Marine Chem.* **21,** 329–345.

Ferdelman T. G., Lee C., Pantoja S., Harder J., Bebout B. M., and Fossing H. (1997) Sulfate reduction and methanogenesis in a Thioploca-dominated sediment off the coast of Chile. *Geochim. Cosmochim. Acta* **15,** 3065–3079.

Ferdelman T. G., Fossing, H., Neumann, K., and Schulz, H. D. (1999) Sulfate reduction in surface sediments of the south-east Atlantic continental margin between 15°38′S and 27°57′S (Angola and Namibia). *Limnol. Oceanog.* **44,** 650–661

Fossing H. (1990) Sulfate reduction in shelf sediments in the upwelling region off Central Peru. *Cont. Shelf Res.* **10,** 355–367.

Fossing H. and Jørgensen B. B. (1989) Measurement of bacterial sulfate reduction in sediments: Evaluation of a single-step chromium reduction method. *Biogeochem.* **8,** 205–222.

Fossing H. and Jørgensen B. B. (1990) Oxidation and reduction of radiolabeled inorganic sulfur compounds in an estuarine sediment, Kysing Fjord, Denmark. *Geochim. Cosmochim. Acta* **54,** 2731–2742.

Hansen L. B., Finster K., Fossing H., and Iversen N. (1998) Anaerobic methane oxidation in sulfate depleted sediments: Effects of sulfate and molybdate additions. *Aqua. Microb. Ecol.* **14,** 195–204.

Heggie D. T., Skyring G. W., O'Brien G. W., Reimers C., Herczeg A., Moriarty D. J. W., Burnett W. C., and Milnes A. R. (1990) Organic carbon cycling and modern phosphorite formation on the East Australian continental margin: An overview. In *Phosphorite Research and Development* (eds. A. J. G. Notholt and I. Jarvis). *Geol. Soc. Spec. Pub.* **52,** 87–117.

Hoehler T. M., Alperin M. J., Albert D. B., and Martens C. S. (1994) Field and laboratory studies of methane oxidation in an anoxic marine sediment: Evidence for a methanogen-sulfate reducer consortium. *Global Geochem. Cyc.* **8,** 451–463.

Iversen N. and Jørgensen B. B. (1985) Anaerobic methane oxidation rates at the sulfate-methane transition in marine sediments from Kattegat and Skagerrak (Denmark). *Limnol. Oceanog.* **30,** 944–955.

Iversen N. and Jørgensen B. B. (1993) Diffusion coefficients of sulfate and methane in marine sediments: Influence of porosity. *Geochim. Cosmochim. Acta* **57,** 571–578.

Jannasch H. W. and Taylor C. D. (1984) Deep-sea microbiology. *Ann. Rev. Microb.* **38,** 487–514.

Jahnke R. A., Emerson S. R., Reimers C. E., Schuffert J., Ruttenberg K., and Archer (1989) Benthic recycling of biogenic debris in the eastern tropical Atlantic Ocean. *Geochim. Cosmochim. Acta* **53,** 2747–2960.

Jørgensen B. B. (1978) A comparison of methods for the quantification of bacterial sulfate reduction in coastal marine sediments. I. Measurements with radiotracer technique. *Geomicrobio. J.* **1,** 11–27.

Jørgensen B. B. (1983) Processes at the sediment-water interface. In *The Major Biogeochemical Cycles and their Interactions* (eds. B. Bolin and R. B. Cook). Chap. **18,** pp. 477–509. SCOPE

Jørgensen B. B. (1989) Sulfate reduction in marine sediments from the Baltic Sea—North Sea transition. *Ophelia.* **31,** 1–15.

Jørgensen B. B. and Fenchel T. (1974) The sulfur cycle of a marine model system. *Mar. Biol.* **24,** 189–201.

Martens C. S. and Berner R. A. (1977) Interstitial water chemistry of Long Island Sound. I. Dissolved gases. *Limnol. Oceanog.* **22,** 10–25.

Martens C. S., Albert D. B., Alperin M. J., Taylor E. J., and Clesceri E. J. (1998) Shipboard and in situ measurements of sulfate reduction

in upper slope sediments at 35°20′N to 35°25′N north of Cape Hatteras, NC (USA). *EOS, Trans. AGU Ocean Sci. Meeting Suppl.* **79,** 0S183.

Middelburg J. J., Soetaert K., and Herman P. M. J. (1997) Empirical relationships for use in global diagenetic models. *Deep-Sea Res.* **44,** 327–344**.**

Nickerson C. R. (1978) Consolication and permeability characteristics of deep sea sediments: North central Pacific Ocean. MSc Thesis, Worcester Polytechnic Institute, Massachusetts

O'Hara S.C.M., Dando P. R., Schuster U., Bennis A., Boyle J. D., Chui F. T. W., Hatherell V. J., Niven S. J., and Taylor L. J. (1995) Gas seep induced interstitial water circulation: Observation and environmental implications. *Cont. Shelf Res.* **15,** 931–948.

Niewöhner C., Hensen C., Kasten S., and Schulz H. D. (1998) Deep sulfate reduction completely mediated by anaerobic methane oxidation in sediments of the upwelling area off Namibia. *Geochim. Cosmochim. Acta* **62,** 455–464.

Parkes R. J., Cragg B. A., Getliff J. M., Harvey S. M., Fry J. C., Lewis C. A., and Rowland S. J. (1993) A quantitative study of microbial decomposition of biopolymers in recent sediments from the Peru Margin. *Mar. Geol.* **113,** 55–66.

Parkes R. J., Cragg B. A., Bale S. J., Getliff J. M., Goodman K., Rochelle P. A., Fry J. C., Weightman A. J., and Harvey S. M. (1994) Deep bacterial biosphere in Pacific Ocean sediments. *Nature* **371,** 410–413.

Pelegri S. P., Nielsen L. P., and Blackburn T. H. (1994) Denitrification in estuarine sediment stimulated by the irrigation activity of the amphipod Corophium volutator. *Mar. Ecol. Prog. Ser.* **105,** 285–290.

Pimenov N., Davidova I., Belyaev S., Lein A., and Ivanov M. (1993) Microbial processes in marine sediments in the Zaire river delta and the Benguela upwelling region. *Geomicrobio. J.* **11,** 157–174.

Pruysers P. A. (1998) Early diagenetic processes in sediments of the Angola Basin, eastern South Atlantic. Ph.D. dissertation, Univ. Utrecht.

Romero-Wetzel M. B. (1987) Sipunculans as inhabitants of very deep, narrow burrows in deep-sea sediments. *Mar. Biol.* **96,** 87–91.

Rowe G. T. and Deming J. W. (1985) The role of bacteria in the turn over of organic carbon in deep-sea sediments. *J. Marine Res.* **43,** 925–950.

Rowe G. T. and Howarth R. (1985) Early diagenesis of organic matter in sediments off the coast of Peru. *Deep-Sea Res.* **32,** 43–55.

Schneider R., Dahmke A., Kölling A., Müller P. J., Schulz H. D., and Wefer G. (1992) Strong deglacial minimum in the $\delta^{13}C$ record from planktonic foraminifera in the Benguela upwelling region: Palaeoceanographic signal or early diagenetic imprint? In, *Upwelling Systems: Evolution Since the Early Miocene* (eds. C. P. Summerhayes, W. L. Prell, and K. Emeis) *Geol. Soc. Spec. Pub.* **64,** 285–297.

Schulz H. D., Dahmke A., Schinzel U., Wallmann K., and Zabel M. (1994) Early diagenetic processes, fluxes, and reaction rates in sediments of the South Atlantic. *Geochim. Cosmochim. Acta* **58,** 2041–2060.

Schulz H. D. and Cruise praticipants (1996) Report and preliminary results of Meteor Cruise M 34/2, Walvis Bay—Walvis Bay, 29.1.—18.2.1996. *Berichte aus dem Fachbereich Geowissenschaften der Universität Bremen* No. 78.

Skyring G. W. (1987) Sulfate reduction in coastal ecosystems. *Geomicrobio. J* **5,** 295–374.

Thamdrup B., Fossing H., and Jørgensen B. B. (1994) Manganese, iron, and sulfur cycling in a coastal marine sediment, Aarhus Bay, Denmark. *Geochim. Cosmochim. Acta* **23,** 5115–5129.

Thode-Andersen S. and Jørgensen B. B. (1989) Sulfate reduction and formation of ^{35}S-labelled FeS, FeS_2, and S^o in two coastal sediments. *Est. Coast, and Shelf Sci.* **15,** 255–266.

Thomson J. and Wilson T. R. S. (1980) Burrow-like structures at depth in a Cape Basin red clay core. *Deep-Sea Res.* **27A,** 197–202.

Wang Y. and van Cappelen P. (1996) A multicomponent reactive transport model of early diagenesis: Application to redox cycling in coastal marine sediments. *Geochim. Cosmochim. Acta* **60,** 2993–3014.

Weaver P. P. E. and Schultheiss P. J. (1983) Vertical open burrows in deep-sea sediments 2 m in length. *Nature* **310,** 329–331.

Wefer G. and Cruise participants (1988) Bericht über die METEOR-Fahrt M 6/6, Libreville—Las Palmas, 18.2—23.3.1988. *Berichte aus dem Fachbereich Geowissenschaften der Universität Bremen* No. 4.

Wetzel A. (1981) Ökologische und stratigraphische Bedeutung biogener Gefüge in quartären Sedimenten am NW-afrikanischen Kontinentalrand. *Meteor Forschungsergebnisse Reihe C* **34,** 1–47.

Widdel F. (1988) Microbiology and ecology of sulfate- and sulfur-reducing bacteria. In *Biology of Anaerobic Microorganisms* (ed. A. B. J. Zehnder). Chap. **10,** pp. 469–585 John Wiley & Sons, NY.

Yamamoto S., Alcauskas J. B., and Crozier T. E. (1976) Solubility of methane in distilled water and seawater. *J. Chem. Eng. Data* **21,** 78–80.